APRIL 15 2025

Long-range propagation of airgun-array signals: Comparing numerical simulations and acoustic recordings in the Ionian sea

Alice Affatati ; Federica Pace; Michael Wood; Salvatore Viola; Beatrice Maria Perla Galante; Virginia Sciacca; Cécile Ducatel; Mireille Laigle; Giorgio Riccobene; Davide Embriaco; Francesco Simeone; Giuditta Marinaro; Fabio Romanelli; Roberto Racca; Angelo Camerlenghi

J. Acoust. Soc. Am. 157, 2857–2867 (2025)
https://doi.org/10.1121/10.0036457

JASA ARTICLE

Long-range propagation of airgun-array signals: Comparing numerical simulations and acoustic recordings in the Ionian sea

Alice Affatati,[1,2,3,a] Federica Pace,[4] Michael Wood,[5] Salvatore Viola,[6] Beatrice Maria Perla Galante,[2] Virginia Sciacca,[7] Cécile Ducatel,[8] Mireille Laigle,[9] Giorgio Riccobene,[6] Davide Embriaco,[10] Francesco Simeone,[10] Giuditta Marinaro,[10] Fabio Romanelli,[1] Roberto Racca,[11] and Angelo Camerlenghi[2,3]

[1]*Department of Mathematics, Informatics and Geosciences, University of Trieste, Trieste, 34128, Italy*

[2]*National Institute of Oceanography and Applied Geophysics–OGS, Trieste, 34010, Italy*

[3]*Jean Monnet Centre of Excellence on Sustainable Blue Economy, Euro-Mediterranean University EMUNI, Piran, Slovenia*

[4]*JASCO Applied Sciences (Deutschland) GmbH, 24223, Schwentinental, Germany*

[5]*JASCO Applied Sciences (UK) Ltd., Droxford, Hampshire, SO32 3PW, United Kingdom*

[6]*INFN, Laboratori Nazionali del Sud, Via S. Sofia 62, Catania, 95123, Italy*

[7]*Istituto di Scienze Polari-Consiglio Nazionale delle Ricerche (CNR-ISP), 98122, Messina, Italy*

[8]*REM/GM, Centre de Brest, Institut Français de Recherche pour l'Exploitation de la MER, IFREMER, 29280, Plouzané, France*

[9]*Geoazur, Université de la Côte d'Azur, CNRS, Observatoire de la Côte d'Azur, IRD, F-06560 Valbonne, France*

[10]*National Institute of Geophysics and Volcanology, INGV, Rome, Italy*

[11]*JASCO Applied Sciences (Canada) Ltd., Victoria, British Columbia, V8Z 7X8, Canada*

ABSTRACT:
Marine seismic surveys contribute to acoustic pollution, and the sounds they produce may be audible by marine mammals at several hundred kilometers distance. To evaluate the potential effects of such sounds on fauna and translate them into effective policies and mitigation measures, stakeholders require quantitative estimations of acoustic fields. We compare simulations of airgun-array signals produced during the Upper LIthosphere Ship Subduction Exploration survey in the Ionian Sea with the signals recorded 650 kilometers away at the cabled seabed observatory NEMO-SN1. JASCO's Applied Sciences' Airgun Array Source Model was used to predict the sound levels for two configurations of 18-element airguns, and the signal was then propagated in a realistic environment utilizing JASCO's Full-Waveform Range dependent Acoustic Model from the source to the position of the receiver station. There is a qualitative agreement between the simulated, denoised, and recorded signals of the airgun arrivals. However, the signal simulated at 650 kilometers from the source stretches and shows fewer high-frequency components compared to the received one. Our study quantitatively shows that the peaks produced by a large airgun array during a scientific cruise, at 160–180 Hz are not masked by ambient noise even in busy shipping locations at a distance of 650 km.
 https://doi.org/10.1121/10.0036457

(Received 9 August 2024; revised 4 March 2025; accepted 31 March 2025; published online 15 April 2025)

[Editor: Julien Bonnel] Pages: 2857–2867

I. INTRODUCTION

Marine seismic surveys are a fundamental tool in geological research, geohazard characterization, and resource exploration; they do, however, contribute heavily to acoustic pollution in terms of energy and ranges of influence in time and space domains (Duncan *et al.*, 2017; Nowacek *et al.*, 2015; Przeslawski *et al.*, 2018).

Seismic surveys generally use impulsive sources known as airguns (Caldwell and Dragoset, 2000; Gisiner, 2016; Ziolkowski *et al.*, 1982). Airguns rapidly release compressed air stored in a chamber, generating high-amplitude, low-frequency acoustic signals that ensonify the seabed, enabling an analysis of the sea bottom properties from the return signal (e.g., Dragoset, 2000; McCauley *et al.*, 2021).

[a]Email: aaffatati@ogs.it

Airguns are generally used in arrays with volumes, characteristics, position, and a number of elements varying according to the aim of the seismic survey (Caldwell and Dragoset, 2000; Dragoset, 1990, 2000; Martin *et al.*, 2017; Prior *et al.*, 2021). Although airgun arrays are configured to direct most of the acoustic energy toward the sea bottom, a considerable amount of energy is also emitted horizontally (Nieukirk *et al.*, 2004). Airgun array signals may still be detectable above the background noise levels at low frequencies hundreds of km away from the source (Blackwell *et al.*, 2015; Bohnenstiehl *et al.*, 2012; MacGillivray *et al.*, 2014; Martin *et al.*, 2017; Prior *et al.*, 2021). For this reason, numerical simulations investigating long-range propagations are critically important for environmental impact assessment (e.g., Nowacek *et al.*, 2015), whereas most scientific research focuses on analyzing close-range effects (Affatati and Camerlenghi, 2023).

The sound produced by seismic surveys can affect marine fauna (e.g., Duncan *et al.*, 2017; Gisiner, 2016; Affatati, 2020; McCauley *et al.*, 2021), and there is an urgency to understand the potential effects of seismic operations on different marine taxa (Carroll *et al.*, 2017). Scientists, policymakers, and other stakeholders require more information related to quantitative estimation of the acoustic field produced by airguns and airgun arrays (e.g., Ainslie *et al.*, 2016; Directive 2008/56/EC, European Union, 2008; National Marine Fisheries Service, 2018; Sigray *et al.*, 2023; Southall *et al.*, 2023).

Here, we simulated airgun array signals for the Upper LIthosphere Ship Subduction Exploration (ULYSSE) research seismic survey conducted in the Aegean Sea in November 2012. We compared the simulated signals with acoustic recordings at the Neutrino Mediterranean Observatory—Submarine Network 1 (NEMO-SN1), which is located in the Western Ionian Sea, off Eastern Sicily, ∼650 km from the area where the seismic survey was conducted (Favali *et al.*, 2013). Since airgun arrays are not point sources (Ainslie *et al.*, 2016) and thus exhibit directivity properties dependent on their geometry, we performed source modeling for two configurations of arrays, and we conducted a computational long-range propagation of the seismic signals. Most of the available studies on the effect of seismic surveys on fauna focus on shorter-distance propagations (Affatati and Camerlenghi, 2023). To the best of our knowledge, no other studies have evaluated the propagation of airgun-array signals over distances of >500 kilometers, apart from Heaney and Campbell (2019) who investigated the basin acoustic field for the array at a maximum range of 400 km. Numerical simulations are powerful tools to analyze the generation and propagation of underwater sound, but their predictions may disagree with results from experimental measurements (Aerts and Streever, 2016). The results presented in this work highlight the relevance of modeling the propagation of airgun-array sounds in complex environments and the paramount importance of validating the models with experimental data. Such information is crucial for understanding the impact of seismic surveys on marine mammals and the ecosystem and implementing effective mitigation strategies. Whale activities (e.g., migration, traveling, socializing) can lead to different exposure effects that include displacement from an area, with possible long-term detrimental effects at the population level, a condition that has not yet been entirely understood. The Mediterranean sub-population of fin whales (*Balaenoptera physalus*) present in our study area is considered "endangered" by the International Union for Conservation of Nature (IUCN) Red List of Threatened Species (Cooke, 2018), and can be especially affected by anthropogenic noise sources due to its low-frequency sensitivity (Sciacca *et al.*, 2016; Sciacca *et al.*, 2023). For example, fin whales may leave an area with seismic airgun activity for an extended period (Castellote *et al.*, 2012). In light of the findings of this study, it is of great importance to better assess anthropogenic impacts through experiments involving all relevant stakeholders to achieve a more refined understanding of the behavioral response (Southall *et al.*, 2023). In particular, the long-range propagation on the order of hundreds of kilometers should be introduced in future studies, when applicable, in order to provide policymakers with improved information to implement efficient mitigation tools (Aerts and Streever, 2016; Ainslie *et al.*, 2016).

II. MATERIALS AND METHODS

A. Scientific cruise and study area

The ULYSSE cruise was conducted in the Aegean Sea between November 4 and 20, 2012, using the scientific research French vessel N/O POURQUOI PAS? co-funded by the Institut Français de Recherche pour l'Exploitation de la MER (IFREMER) and the French Navy (IMO:9285548 Global class, IFREMER, 2012). Figure 1 shows the seismic survey area and the location of the NEMO-SN1 observatory where the propagated signals were measured.

The primary aim of the ULYSSE deep-penetration survey was to analyze the megathrust fault and the outer forearc domain of the South-West segment of the Hellenic subduction zone (ULYSSE Cruise Report, 2012, unpublished, see https://campagnes.flotteoceanographique.fr/campagnes/12030100/) using seismic reflection and refraction techniques (Laigle and Sachpazi, 2012).

B. Airgun array configurations

The ULYSSE survey was performed using two different configurations of 18-element airgun arrays with total volumes of 11 441 and 8867 in.^{3} for refraction and reflection studies, respectively. The arrays were towed at three different depths (18, 22, and 26 m). It is worth noting that the

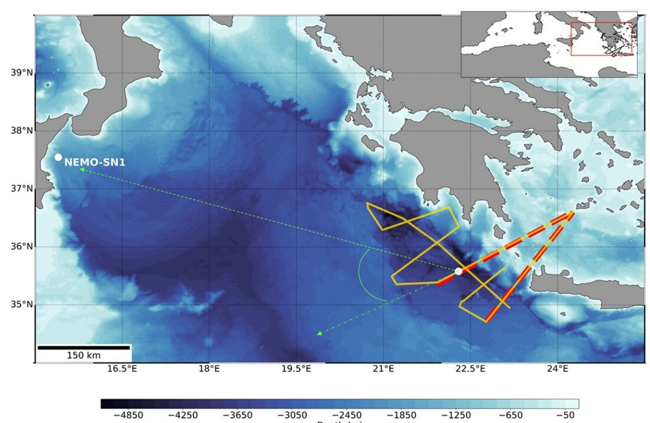

FIG. 1. Map of the study area showing the location of the NEMO-SN1 observatory (Latitude 37.5477° N, Longitude 15.3975° E) and the ULYSSE survey (Laigle and Sachpazi, 2012). The yellow lines indicate the reflection survey and the orange dashed lines the refraction survey. The unlabeled white dot shows the location of the source. The green dotted lines represent the ship heading and the bearing (54.25°) used in the simulations. The track data for the ship route was downloaded from SISMER IFREMER (https://donnees-campagnes.flotteoceanographique.fr/search; '201203010055.nvi' file).

11 441 in.[3] configuration presents an asymmetrical airgun geometry. See supplementary material.

C. Numerical simulations

Airgun-array signals were modeled for both configurations using JASCO's Airgun Array Source Model (AASM; MacGillivray, 2006, 2019) and propagated with JASCO's Full Waveform Range-dependent Acoustic Model (FWRAM; Matthews and MacGillivray, 2013).

A model validation using data recorded at the NEMO-SN1 deep-cable observatory was conducted at the end of the simulations (for a detailed description of data acquisition and model validation, see Secs. II D–II F).

1. Source generation

The acoustic signatures and surface-affected source spectrum (ISO, 2017) for both configurations of the arrays (see the supplementary material for a detailed description of the airgun-array configurations, SuppPub1) were computed using AASM. AASM simulates acoustic pressure waveforms for the individual airguns in the array based on their volume, tow depth, and pressure, also accounting for the elements' interactions (Matthews and MacGillivray, 2013; Racca and Scrimger, 1986). AASM includes both a low-frequency and a high-frequency module for predicting different components of the airgun array spectrum. The low-frequency module is based on the solution of differential equations governing the airgun bubble oscillations (Ziolkowski, 1970) and produces a deterministic output, while the high-frequency module takes small random perturbations in the airgun positions into account to define levels in a stochastic manner. Airgun emissions may have a significant component at high frequencies; AASM uses Monte Carlo simulations to model the random component of the airgun array emission at frequencies above 800 Hz (Ainslie *et al.*, 2016). This model is based on a statistical analysis of an extensive library of high-quality seismic source signature data obtained from the Joint Industry Program on Sound and Marine Life (Mattsson and Jenkerson, 2008).

The parameters used in the source simulation are gun type and positions in the array (X, Y, Z), individual airgun volumes, pressure, and firing delays (see the supplementary material for a detailed description of the airgun-array configurations, SuppPub1).

See supplementary material for the full suite of results for both configurations in the fore-aft and starboard-port directions (SuppPub3).

2. Signal propagation

FWRAM is a sound propagation model based on the parabolic equation algorithm (Collins, 1993) enhanced by using a complex density method (Zhang and Tindle, 1995) which accounts for shear wave losses at the seabed. The complex density approach can accurately model the loss of waterborne acoustic energy due to conversion to shear waves at the seabed interface. This approach avoids potential overestimation of received levels in the water column, especially over long propagation ranges, which could occur for conventional parabolic equation modelling as used in the Heaney and Campbell (2019) study. The output from AASM provides the source waveform from each airgun, which are modelled as individual monopoles. FWRAM employs the array starter method to accurately model sound propagation from the spatially distributed airgun sources (MacGillivray and Chapman, 2012). By summing replicas of the array starter with different phases and ranges, this technique uses the parabolic equation method, accounting for the directionality of the source and allowing for field predictions in the far-field. The environmental parameters used were bathymetry, water sound speed profile, and seabed geoacoustic profile, including a three-layered structure consisting of silty sand and halite; see the supplementary material for a detailed description of the environmental parameters used for the acoustic propagation (SuppPub2).

The ship track bearing is 237.25° and the bearing from the source to the receiver is 291.5° (Fig. 1). The geographical coordinates of the source to be propagated (white unlabeled dot) were chosen as a point in the deepwater Hellenic trench where the refraction and reflection seismic profiles overlap.

The main parameters used for the simulation are shown in Table I.

D. Cabled deep-sea seafloor observatory

Acoustic data were recorded during ULYSSE at the NEMO-SN1 cabled observatory (Favali *et al.*, 2013).

NEMO-SN is located in the Western Ionian Sea off Eastern Sicily and consists of two different platforms: the SN1 abyssal station and the OνDE abyssal acoustic station. The whole system is connected and powered from the shore with a 25-km long electro-optical cable and is synchronized with a global positioning system (GPS) and connected in real-time with the shore laboratory. At the time of the survey, the infrastructure was jointly operated by Istituto Nazionale di Geofisica e Vulcanologia (INGV) and Istituto Nazionale di Fisica Nucleare (INFN).

TABLE I. Values used to run the simulation.

Parameter	Value
Array bearing	54.25°
Min frequency (Hz)	2.0
Max frequency (Hz)	200
Frequency step	0.05
Max output range (m)	650 000
Target output depth (m)	2000
Range resolution (m)	$f \leq 80$ Hz: 50 $f > 80$ Hz: 25
Depth resolution (m)	$f \leq 10$ Hz: 2.5 $f \leq 50$ Hz: 1.25 $f \leq 80$ Hz: 1.0 $f \leq 160$ Hz: 0.5 $f > 160$ Hz: 0.25

The SN1 real-time cabled seafloor observatory operated at a depth of 2100 m in the Western Ionian Sea, off Eastern Sicily, Italy (Latitude 37.5477° N, Longitude 15.3975° E, Viola *et al.*, 2017) between 2012 and 2013. The cabled seafloor observatory located approximately 650 kilometers away from the source during the ULYSSE survey (Fig. 1) performed long-term monitoring to acquire acoustic, oceanographic, geophysical, and environmental measurements. This observatory was the first node of the European Multidisciplinary Seafloor Observatory (EMSO ERIC, https://emso.eu/).

E. Acoustic data acquisition

The acoustic recordings used in this study were acquired using the SMID DT405D(V)1 seismic hydrophone (average sensitivity of -197 ± 1 dB re 1 V/μPa in the frequency range 50 mHz–1 kHz; Viola *et al.*, 2017). The frequency response of the ceramic sensor, measured experimentally in the band from 40 Hz to 1 kHz, is almost flat at -197 ± 1 dB re 1 V/μPa. It is reasonable to think that it remains flat even at lower frequencies, down to the order of Hz. At 500 Hz, the sensor response is omnidirectional within 2 dB. First, the signal was digitized offshore (sampling rate of 2 kHz); then, it was sent to the onshore station connected through a 28-km-long optical link. A GPS receiver was used to provide absolute time synchronization with millisecond accuracy. The acquired data were stored in 10-min-long files before processing (Favali *et al.*, 2013). Acoustic signals were acquired through two acquisition channels at 12 bits by using two different gains (+30 and +60 dB). The high gain acquisition channel was used for the airgun signal analysis presented in this work. The absolute time of acquisition is embedded in each file, and it was transmitted to the underwater observatory by the GPS receiver installed in the shore station.

F. Comparison between simulation and acoustic recordings

The simulation for the 8867 in.^{3} configuration was compared to acoustic data recorded by NEMO-SN1 in a half-hour period around the chosen time for the simulation. In order to isolate the contribution of the airguns from the diffuse background acoustic noise, a denoising method was applied. The spectrogram of each pulse was calculated over a 20 s window and the maximum value of the power spectral density (PSD) in each frequency bin -computed between 8 and 7 s before the main pulse -was subtracted from the whole time window.

Sound exposure level (SEL, dB re 1 μPa^2 s) plots were also produced for the synthetic signal and the denoised recorded signal using a 20 s window.

III. RESULTS

A. Modeled surface-affected source waveform and spectral densities

Figure 2 shows the simulated surface-affected source waveform and the source SEL spectral density (dB re 1 μPa^{2}m^{2}s/Hz) for the 8867 in.^{3} (a) and 11 441 in.^{3} arrays (b), respectively, at a bearing of 54.25° resulting from the difference between the towing direction of the array (237.25°) and the direction of propagation towards the NEMO-SN1 observatory (291.5°) (see Fig. 1).

As shown in Fig. 2, both airgun signals are consistent with the source waveforms that one would expect based on theory (Ainslie *et al.*, 2016; ISO, 2017). The combined expanding and collapsing of bubbles results in a series of consecutive peaks in the low frequency (Fig. 2, Prior *et al.*, 2021). The signal then decays within 1000 ms.

The frequency content of the array indicates a sound exposure source level spectral density peak (~220 dB re 1 μPa^{2}m^2 s/Hz) at ~10 Hz and a frequency content lowering to 100–120 dB re 1 μPa^{2}m^2 s/Hz at 10 000 Hz. The energy useful for geophysical prospecting is generally low frequency (i.e., < 100 Hz); however, the simulated spectra show energy persistent to several kHz.

The azimuthal directivity analysis (see the supplementary material for the full suite of results for both configurations in the fore-aft and starboard-port directions, SuppPub3) indicates significant focusing of the emitted energy in the fore-aft direction only in the frequency band ~15–30 Hz for the 8867 in.^{3} array.

See the supplementary material for the full suite of results for both configurations in the fore-aft and starboard-port directions (SuppPub3). In this work, we are not concerned with simulating the airgun array signal in the vertical direction since this component, while essential for geophysical prospecting purposes, is of little relevance to long-range environmental noise. We instead focus on the horizontal propagation of the signal in the direction of NEMO-SN1, which is critical for understanding the effects on marine fauna. From now on, we will consider the 8867 in.^{3} configuration.

B. Signal propagation

The synthetic signal for the 8867 in.^{3} array configuration was propagated to 650 km from the source in the direction of the receiving station NEMO-SN1 (Fig. 1) using FWRAM. The sound propagation along the transect of interest was modeled for individual frequencies from 2.0 to 200 Hz, with a frequency spacing of 0.05 Hz (Table I). The time domain realization of the signal was obtained through an inverse Fourier transform of the model outputs resulting in a received signal of 20.0 s at the target receiver location. The waveform is shown in Fig. 3.

Low-amplitude precursors precede the main peak, which entails a series of high-amplitude oscillations with maximum negative-amplitude peaks followed by a long tail of lower-amplitude oscillations. After propagation at 650 km, the surface-affected source waveform with a duration of approximately 1 s is stretched to approximately 5 s. The long tail of lower amplitude oscillations, probably due to the dispersive nature of the propagation channel, does not allow the precise identification of the duration of the

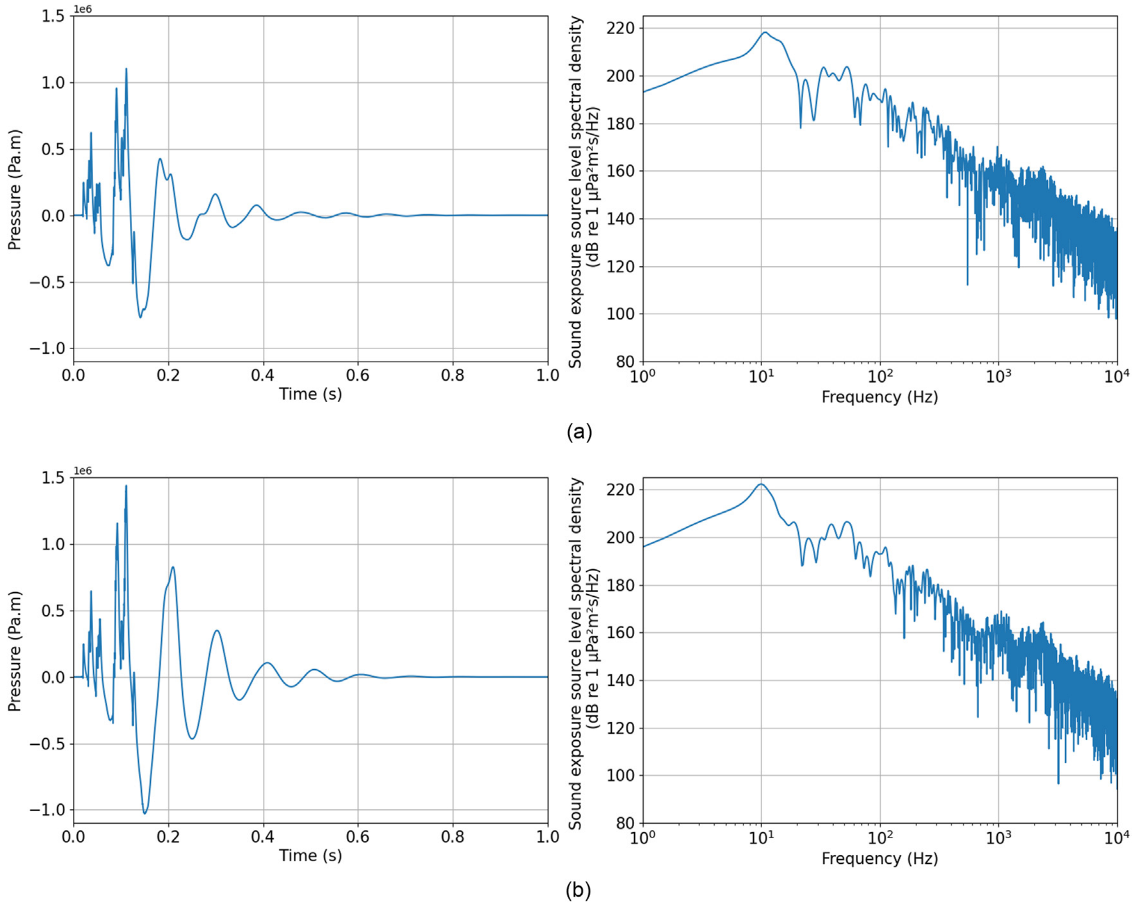

FIG. 2. Source waveforms (left panels) and sound exposure source level spectral density (right panels) simulated with AASM for (a) 8867 in.[3] and (b) 11 441 in.[3] configurations at a bearing of 54.25° resulting from the difference between the towing direction (237.25°) and the direction of propagation towards the NEMO-SN1 observatory (291.5°).

propagated signal. In fact, broadband signals at the source can transform into longer-duration, frequency-modulated sounds at a distance of several kilometers, or more, from the source itself (e.g., Erbe *et al.*, 2016).

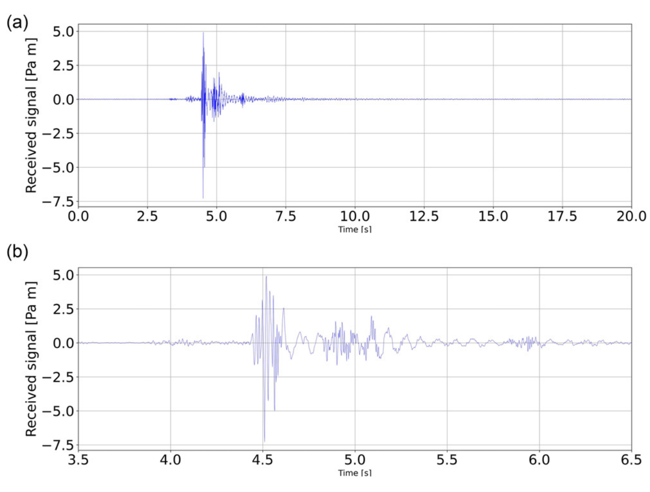

FIG. 3. Synthetic signal calculated at 650 km from the source (location of the NEMO-SN1 hydrophone placed at 2000 m depth) for the 8867 in.[3] array configuration; (a) in a 20 s window, and (b) zoomed-in version in a 3 s window.

C. Measured signal

Figure 4 shows spectrograms computed with 30 min of acoustic data (from 16:40 to 17:10 UTC on November 6, 2012), corresponding with the time chosen for the simulation; the recordings at NEMO-SN1 were obtained throughout the duration of the ULYSSE survey. The signals of the 8867 in.[3] airgun configuration appear clearly in the lower-frequency portion of the spectrogram with an inter-pulse interval of 60 s. The frequency content and intensities of individual pulses appear highly variable. Marked signal variability above approximately 100 Hz is clearly shown in Fig. 4(b).

Tonal components and pseudo-harmonics are clearly visible between about 10 Hz and 100 Hz (Fig. 4b; Guerra *et al.*, 2009). This structure appears continuous during the 30-min recording interval.

The spectrogram also shows that the highest intensity peaks of the airgun arrivals are centered around 10 Hz. The high-intensity 10 Hz signal does not appear to decay between the pulses, and it is still present at the arrival of the following received pulse.

NEMO-SN1 is located on a shipping route. The ship traffic density during the survey period was already shown by Viola *et al.* (2017) who analyzed automated identification system (AIS) data (Fig. 5).

https://doi.org/10.1121/10.0036457

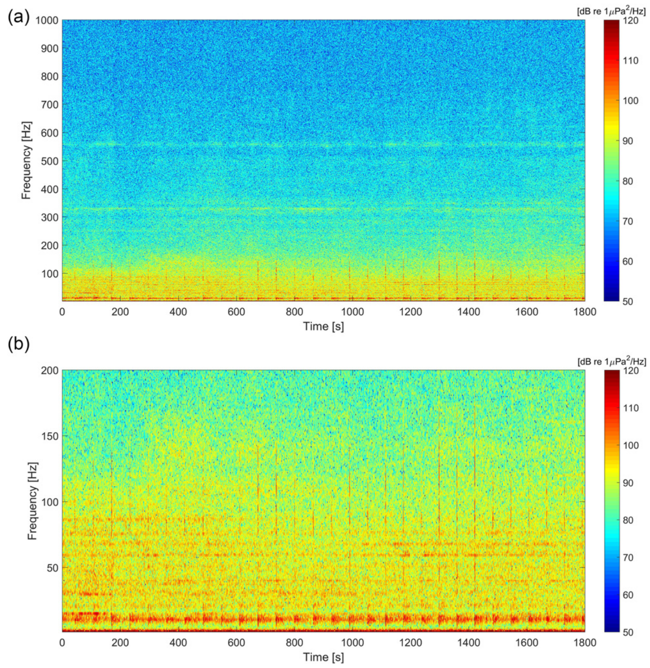

FIG. 4. Spectrograms of acoustic recordings with airgun pulses at NEMO-SN1 computed with 2048-point fast Fourier transform, Hanning window, and 98% overlap (30-min recording from 16:40 to 17:10 UTC on November 6, 2012). (a) Full-scale version of the spectrogram up to 1 kHz; (b) zoomed-in version of the spectrogram up to 200 Hz.

A spectrogram showing the beginning of the airgun survey is shown in Fig. 6 (∼1000 s from the start of the recordings). The first airgun array signals are audible at the site on November 6, later with respect to the real start of the survey.

D. Comparison between simulation and acoustic recordings

Figure 7(a) shows the average spectrogram of the pulses recorded by the NEMO-SN1 in a half-hour period around the time considered in the simulation (November 6, 2012, 16:30 UTC). The average spectrogram of the pulses was computed after temporally aligning the recorded pulses using cross-correlation. The spectrogram was calculated by downsampling the recorded signals at 400 Hz—the sampling frequency used in the simulation—and by applying a fast Fourier transform at 256 points on a 99% overlapped time window.

Figure 7(b) shows the mean values of the denoised spectrograms related to all pulses recorded by the NEMO-SN1 station in a half-hour. We still see the presence of the 10 Hz tail after the airgun's main peak. This low-frequency component appears entirely attenuated during the few seconds preceding the airgun signal by the denoising method. The high-intensity maxima (10 Hz and its pseudo-harmonics) are not entirely attenuated by denoising.

Figure 7(c) shows the spectrogram of the simulated airgun signal after propagation of 650 km. The long tail of energy centered on approximately 10 Hz is also visible in this spectrogram, and a weaker low-frequency signal component appears to be constant before the first airgun arrival. The high-intensity frequency bands of the airgun arrival (e.g., 30–60 and 80–120 Hz) coincide with the residual intensities in the same frequency bands before and after the airgun signal. Two frequency notches are visible, centered at approximately 30 and 70 Hz. The higher frequency contents (above ∼120 Hz) that are typical of the airgun impulses in the experimental data [Figs. 7(a) and 7(b)] are not reproduced in the simulated ones.

We modeled a realistic waveform in a realistic, although approximated, environment at a very long distance from the source, and we found a relatively qualitatively good agreement between the simulated and the recorded data. We also compared the PSD for the recorded signal over a time window of 30 min with the simulated signal (Fig. 8).

The PSDs refer to the percentiles of the average PSD calculated by the Welch method in an 18-s window around each airgun emission detected in half an hour of data. For each emission, the analysis window starts 4 s before the arrival of the most intense pulse, thus it also includes the weakest pulses expected from the simulation. The PSDs of the experimental data are calculated on analysis windows of the same length as those used for the results obtained from the simulation. The percentiles in the figure refer to the

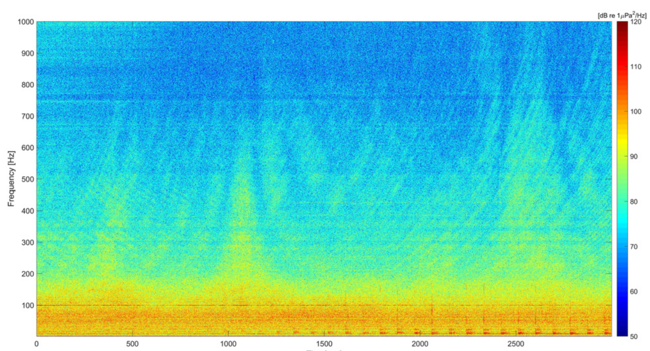

FIG. 5. Typical situation of marine traffic recorded at NEMO-SN1 (Viola et al., 2017). The spectrogram was computed with 4096-point fast Fourier transform, Hanning window, 0.1 s temporal resolution, 0.48 Hz frequency resolution.

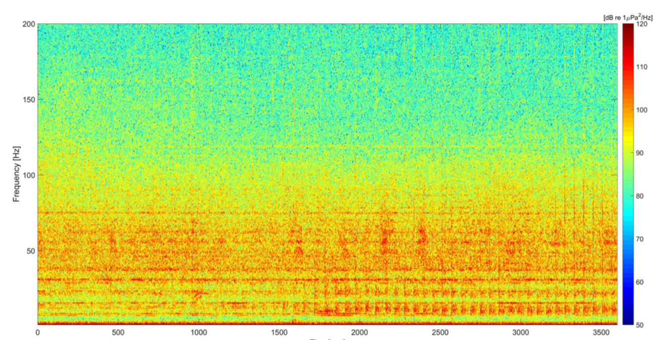

FIG. 6. Spectrogram showing the first airgun array impulses recorded at NEMO-SN1, between 8:40 and 8:50 am on November 6. A 4096-point Fast Fourier Transform, Hanning window was used.

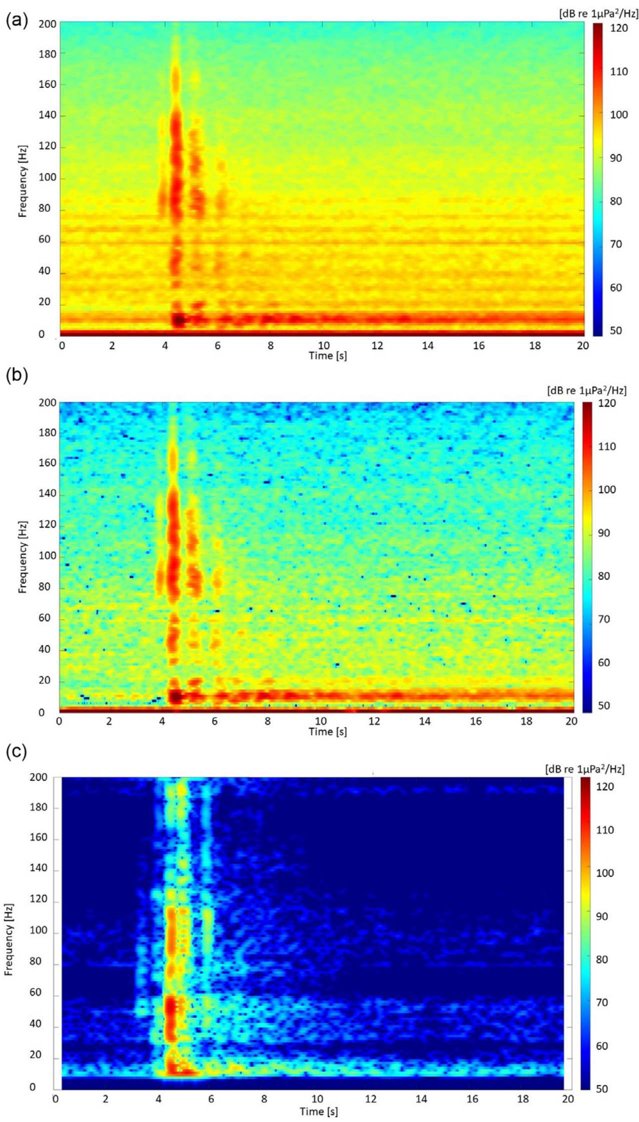

FIG. 7. Panels showing three spectrograms for the 8867 in.^{3} configuration: (a) average of the pulses recorded at NEMO-SN1 without denoising, (b) pulses recorded at NEMO-SN1 with the application of denoising, (c) spectrogram of the simulated signal.

time windows containing airgun pulses and not to the stationary noise. Percentiles were calculated to account for the small variability of the measured airgun signals.

The lowest-frequency portions of the two spectra show the largest difference indicating the contribution of ambient noise. The maximum peak is determined by the arrival of the airgun signal centered at 10 Hz. A secondary peak is present in the simulated signal between 50 and 60 Hz. Conversely, the spectral density that includes the ambient noise is flattened between 15 and 100 Hz and does not show the secondary peak characteristic of the airgun signal.

Figure 9 shows the SEL for the synthetic signal and data recorded at NEMO-SN1, with and without the application of denoising.

In the frequency band 10–200 Hz, the SEL of the recorded data, with or without denoising, is always higher than the simulated one. The only exception is at 50 Hz

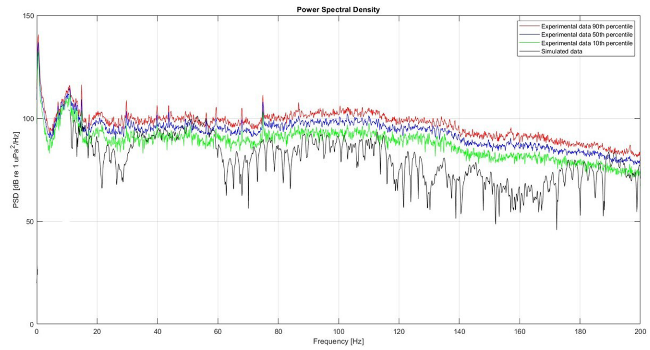

FIG. 8. Comparison between the spectral densities of the simulated and recorded signals at a distance of 650 km from the source. PSD plot of the recorded signal averaged over a time window of 30 min.

where the difference is around 3 dB with respect to the curve related to experimental data, and the experimental SEL with denoising is slightly lower than the simulated one (around 1–2 dB). Outside the band centered around the 50 Hz frequency, the SEL difference between the recorded and synthetic data ranges between 15 and 50 dB re 1 μPa s.

IV. DISCUSSION AND CONCLUSIONS

We modeled the generation and horizontal propagation of the airgun-array signals emitted during the ULYSSE seismic cruise off the western coast of Crete in November 2012. The simulations were compared to data recorded by the NEMO-SN1 cabled observatory located ~650 km from the source.

We analyzed the directivity plots in the horizontal component of both array configurations and simulated the horizontal propagation in the direction linearly connecting the source and the receiver (54.25° with respect to the ship heading). The radiation pattern of the airgun arrays induces source level variations in the vertical and horizontal directions, leading to interactions with the seabed and the water column (Caldwell and Dragoset, 2000). In order to enhance the first bubble pulse and use the low-frequency content (<10–30 Hz) for deep geological targets, the activation of the airguns in the arrays of the ULYSSE cruise was controlled by time delays. These delays have been considered in the source simulation. The resulting radiation pattern of the horizontal component of emitted energy appears to be focused on the fore/aft direction (see the supplementary material for the full suite of results for both ULYSSE airgun configurations, SuppPub3). Therefore, the direction of radiated energy simulated in this study (54.25° with respect to the ship heading) does not represent the maximum horizontal direction of the arrays.

In terms of waveform and frequency spectra, the two array configurations show an unusual signal in which the delays in synchronization generate a maximum amplitude that does not coincide with the first peak, and a relatively long tail of bubble oscillations in the low-frequency range (~10 Hz) (Fig. 2). Overall, the recorded, denoised, and simulated signals of the airgun arrivals are qualitatively similar,

https://doi.org/10.1121/10.0036457

although the simulated signal shows fewer high-frequency arrival levels and not as significant a signal dispersion at 650 km from the source. The simulated signal at 650 km is characterized by the typical signal stretching (∼5 times longer than the source signal) induced by waveguide propagation and the dominance of the 10 Hz frequency component (Fig. 3) typical of the signal's tail. We interpret this tail as the product of the dispersive propagation channel.

In order to better represent the long-range propagation simulated with this study (∼650 km), we used a realistic environment with detailed bathymetry, sound speed profiles in the water column, and acoustic properties of the seabed and subsurface. The correct environmental conditions and the complete array configuration are critical to implementing a more detailed simulation (Ainslie *et al.*, 2016; Duncan *et al.*, 2017). The geoacoustic properties of the subsurface strata used in the simulation include high acoustic impedance contrasts not only between the seabed and the water column but also between the upper silt-sand layer and the underlying salt rock layer typical of the Ionian basin. These lithologic variations contribute to generating multiple waveguides for two-dimensional (2D) signal propagation (McCauley *et al.*, 2000). Additional three-dimensional effects induced by the lateral heterogeneity of the geological environment and by the complex bathymetry of the Ionian basin are not considered in this simulation. These effects may contribute to the differences observed between simulated and recorded data.

A series of continuous pseudo-harmonics of 10 Hz in the recorded data is not present in the simulated data [Figs. 4 and 7(a)]. The origin of these components of the experimental spectrograms, also noted at higher frequencies by Wiggins *et al.* (2016) is uncertain. These structures could be due to tonal components of shipping noise Niu *et al.* (2017). Overall, the recorded, denoised, and simulated signals of the airgun arrivals are qualitatively similar (Fig. 7). The simulated signal in Fig. 7(c) shows fewer high-frequency components. The airgun arrivals displayed in Fig. 4 indicate that there is considerable variability between different arrivals in terms of signal frequency content and level (see also McCauley *et al.*, 2000). In general terms, this variability may be attributed to a combination of source and

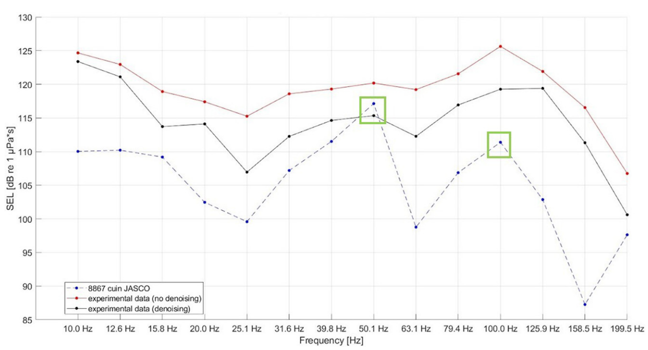

FIG. 9. SEL comparison for recorded data and simulated signal; (a) without denoising, (b) with denoising. Green rectangles show peaks in the modeled airgun-array signal.

propagation effects (e.g., changes in orientation, depth, and functioning of the airguns composing the array) and changes in vessel speed during the survey (Niu *et al.*, 2017). Specifically in relation to the ULYSSE seismic survey, Viola *et al.* (2017) considered the whole NEMO-SN1 dataset (July 2012–April 2013, see Fig. 3 from Viola *et al.*) concluding that intershot variability cannot be related to changes in oceanographic variables. In addition, Vitard (2016) reports severely adverse weather conditions, with winds up to 7 (Beaufort Wind Scale) during the entire cruise, especially in the western sector (outside the Aegean Sea), which is where the recordings and the simulated shot were selected. As a consequence, the entire survey suffered from severe signal quality degradation that influenced negatively, especially the resolution of the seismic reflection data.

While the shots propagating and traveling through the direct path can provide information on the source variability, the propagation on the reflected paths provides insights into the marine environment characteristics. In this case, bathymetry, seabed types and characteristics, surface conditions, and sound speed profiles are the most significant contributors to propagation (Douglass *et al.*, 2024; McCauley *et al.*, 2016).

The spectrogram of the data recorded at the NEMO-SN1 cabled observatory [Fig. 7(a)] outlines the presence of a funnel-shaped tail of energy following each airgun array impulse centered at approximately 10 Hz. This tail appears to be continuous, though decreasing in strength, during the 60 s interval between airgun array arrivals. There is no fading in the signal before the start of the following impulse, as also noticed by Wiggins *et al.* (2016). One preliminary observation from the comparison between modeled and simulated results is that there is an even longer stretching of the original airgun array source signal with respect to the 2D modeling [Fig. 7(c)]. However, the denoising of the recorded signal at NEMO-SN1 cabled observatory removes the 10 Hz at least in the few seconds preceding the arrival of the airgun array source signal [Fig. 7(b)], suggesting that a 10 Hz component overlapping with the tail of the airgun array source signal may be present in the local soundscape or may be due to arrivals from the substrate (Guerra *et al.*, 2009).

We acknowledge some discrepancies between the simulations and the recorded signals (Fig. 7). Our simulations use comprehensive albeit simplified assumptions about the airgun's performance (e.g., uniform energy release). However, we know that adverse weather conditions likely triggered changes in firing pressure and shot-to-shot energy variability and these elements cannot be taken into account in the simulation.

In shallow water, Guerra *et al.* (2011) did not find the same variability we show in Fig. 4 for frequencies above 100 Hz. A lesser degree of variability was also shown in the spectrograms by Camus *et al.* (2021) computed analyzing Seaglider® data. In contrast with these studies, more variability above 100 Hz was shown by Wiggins *et al.* (2016)

and Seri *et al.* (2019). Charif *et al.* (2013) found reverberations between airgun pulses leading to a semi-continuous energy band. Similarly to the deep water of the Gulf of Mexico (e.g., Wiggins *et al.*, 2016), in our study, airgun signals are capable of masking ship traffic below 100 Hz (Fig. 5), and most of the energy is created around 10–100 Hz. Several characteristics of marine environments, such as water depth, play a critical role in affecting received airgun array levels. Each airgun array produces a directional sound field, determined by the array layout. Changes in array layout can be used to reduce the environmental impact of an array (Duncan, 2017; Frisk, 1994). The array used in the ULYSSE survey as modelled in this study shows a high degree of azimuthal directivity (see the supplementary material for the full suite of results for both configurations in the fore-aft and starboard-port directions, SuppPub3). Because the ship course varied substantially during the survey, with prevailing orthogonal directions NW–SE/SE–NW and NE–SW/SW–NE, it is likely that the energy focused in the horizontal direction also varied during the survey. However, this variability should not be reflected in inter-shot variability discussed previously. Additional potential factors influencing pulse length and structure may include the air gun bubble pulse, biophony contributions, and hydrophone vicinity to the seabed (McCauley *et al.*, 2000).

The plot of the SEL as a function of frequency in the range where the airgun array signal dominates (<160–180 Hz) reveals that the de-noising techniques applied reduce the contribution of ambient noise and make the simulated and recorded values more comparable [Fig. 9(b)]. Comparing predicted and measured acoustic data is essential to reduce uncertainties in predicting seismic sources and acoustic outputs (Ainslie *et al.*, 2016; Ainslie *et al.*, 2019; Matthews and MacGillivray, 2013; Prior *et al.*, 2021). The airgun array signals generated by the ULYSSE survey substantially affect the soundscape in the low-frequency range, up to 160–180 Hz (Fig. 4). After traveling ~650 km, the airgun signal in that frequency range exceeds by 10–20 dB the heavy ship traffic background (see Fig. 5). Here, we quantitatively demonstrate that the peaks produced by a large airgun array employed for scientific research at 160–180 Hz are not masked by ambient even in busy shipping locations.

The main long-term goal of this study is to improve the assessment of the effects of airguns on marine fauna. An essential step in evaluating the related risk is to analyze more details of the source used, and its signal propagation, to evaluate the ensonified area that can be used together with the available information on the animal presence and density, and the marine ecosystem (Moretti and Affatati, 2023; Southall *et al.*, 2023).

SUPPLEMENTARY MATERIAL

See the supplementary material for a detailed description of the airgun-array configurations (SuppPub1); a detailed description of the environmental parameters used for the acoustic propagation (SuppPub2); and a full suite of results for both configurations in the fore-aft and starboard-port directions (SuppPub3).

ACKNOWLEDGMENTS

A.A. is funded by the National Institute of Oceanography and Applied Geophysics - OGS, the University of Trieste, and JASCO Applied Sciences. This research is part of the project SONORA ("Filling the gap: Thresholds assessment and impact beyond acoustic pressure level linked to emerging blue-growth activities," under the *JPI Oceans (2022), Joint call for proposals: Underwater Noise in the Marine Environment*, with financial support from the Ministero dell'Università e della Ricerca, CUP identifier F83C22002770006), and Piano Nazionale di Ripresa e Resilienza iNEST Spoke 8: MARITIME, MARINE, AND INLAND WATER TECHNOLOGIES: TOWARDS THE DIGITAL TWIN OF THE UPPER ADRIATIC, Task S8_RT2.1 – Risks and impacts related to chemical contaminants and noise pollution in the hydrosphere, "Modeling of underwater noise pollution for short and long propagation distances." This study has been conducted using E.U. Copernicus Marine Service Information, https://doi.org/10.48670/moi-00021 and the Gibbs Seawater (GSW) Oceanographic Toolbox. A.A. acknowledges the funding by the Jean Monnet Centre of Excellence on Sustainable Blue Economy granted by the European Commission to the Euro-Mediterranean University EMUNI (Grant No. 101048038) in financially supporting this publication. A.A. sincerely thanks Jonathan Mark Ford for the fruitful discussions and encouragement throughout the process of this work. A.A. dedicates this manuscript to Gianni Pavan, who studied cetaceans in the Ionian Sea and supported her during a crucial moment.

AUTHOR DECLARATIONS

Conflict of Interest

The authors declare that they have no conflicts to disclose.

DATA AVAILABILITY

The data that support the findings of this article are available within the supplementary material.

Aerts, L. A., and Streever, B. (**2016**). "Modeled and measured underwater sound isopleths and implications for marine mammal mitigation in Alaska," in *The Effects of Noise on Aquatic Life II* (Springer, New York), pp. 9–16.
Affatati, A. (**2020**). "Underwater noise in the marine environment: Sources, effects on fauna and mitigation measures," Boll. Geofis. Teorica ed Applicata **1**, s1–s110.
Affatati, A., and Camerlenghi, A. (**2023**). "Effects of marine seismic surveys on free-ranging fauna: A systematic literature review," Front. Mar. Sci. **10**, 1222523.
Ainslie, M. A., Halvorsen, M. B., Dekeling, R., Laws, R. M., Duncan, A. J., Frankel, A. S., Heaney, K. D., Küsel, E. T., MacGillivray, A. O., Prior, M. K., Sertlek, H. O., and Zeddies, D. G. (**2016**). "Verification of airgun

sound field models for environmental impact assessment," Proc. Mtgs. Acoust. **27**(1), 070018.
Ainslie, M. A., Laws, R. M., and Sertlek, H. Ö. (**2019**). "International airgun modeling workshop: Validation of source signature and sound propagation models—Dublin (Ireland), July 16, 2016—Problem description," IEEE J. Oceanic Eng. **44**(3), 565–574.
Blackwell, S. B., Nations, C. S., McDonald, T. L., Thode, A. M., Mathias, D., Kim, K. H., Greene, C. R., and Macrander, A. M. (**2015**). "Effects of airgun sounds on bowhead whale calling rates: Evidence for two behavioral thresholds," PLoS One **10**(6), e0125720.
Bohnenstiehl, D. R., Scheip, C. M., Matsumoto, H., and Dziak, R. P. (**2012**). "Acoustics variability of air gun signals recorded at intermediate ranges within the Lau Basin," Geochem. Geophys. Geosyst. **13**, Q11013, https://doi.org/10.1029/2012GC004337.
Caldwell, J., and Dragoset, W. (**2000**). "A brief overview of seismic air-gun arrays," Leading Edge **19**(8), 898–902.
Camus, L., Andrade, H., Aniceto, A. S., Aune, M., Bandara, K., Basedow, S. L., Christensen, K. H., Cook, J., Daase, M., Dunlop, K., Falk-Petersen, S., Fietzek, P., Fonnes, G., Ghaffari, P., Gramvik, G., Graves, I., Hayes, D., Langeland, T., Lura, H., Kristiansen, T., Nøst, O. A., Peddle, D., Pederick, J., Pedersen, G., Sperrevik, A. K., Sørensen, K., Tassara, L., Tjøstheim, S., Tverberg, V., and Dahle, S. (**2021**). "Autonomous surface and underwater vehicles as effective ecosystem monitoring and research platforms in the Arctic—the glider project," Sensors **21**(20), 6752.
Carroll, A. G., Przeslawski, R., Duncan, A., Gunning, M., and Bruce, B. (**2017**). "A critical review of the potential impacts of marine seismic surveys on fish & invertebrates," Mar. Pollut. Bull. **114**(1), 9–24.
Castellote, M., Clark, C. W., and Lammers, M. O. (**2012**). "Acoustic and behavioural changes by fin whales (*Balaenoptera physalus*) in response to shipping and airgun noise," Biol. Conserv. **147**(1), 115–122.
Charif, R. A., Rahaman, A., Muirhead, C. A., Pitzrick, M. S., Warde, A. M., Hall, J., Pyć, C., and Clark, C. W. (**2013**). "Bowhead whale acoustic activity in the southeast Beaufort Sea during late summer 2008–2010," J. Acoust. Soc. Am. **134**(6), 4323–4334.
Collins, M. D. (**1993**). "A split-step Padé solution for the parabolic equation method," J. Acoust. Soc. Am. **93**(4), 1736–1742.
Cooke, J. G. (**2018**). "*Balaenoptera physalus*, The IUCN red list of threatened species 2018: E.T2478A50349982," https://www.iucnredlist.org/species/2478/50349982 (Last viewed February 10, 2024).
Douglass, A. S., Abadi, S., Wood, W. T., and Phrampus, B. J. (**2024**). "A quantitative analysis of acoustic field directionality from a seismic airgun array," Geophysics **89**(6), V653–V667.
Dragoset, B. (**2000**). "Introduction to air guns and air-gun arrays," Leading Edge **19**(8), 892–897.
Dragoset, W. H. (**1990**). "Air-gun array specs: A tutorial," Leading Edge **9**(1), 24–32.
Duncan, A. J. (**2017**). "Airgun arrays for marine seismic surveys-physics and directional characteristics," in *Proceedings of the Acoustics 2017*, Perth, Australia, p. 10.
Duncan, A. J., Weilgart, L. S., Leaper, R., Jasny, M., and Livermore, S. (**2017**). "A modelling comparison between received sound levels produced by a marine Vibroseis array and those from an airgun array for some typical seismic survey scenarios," Mar. Pollut. Bull. **119**(1), 277–288.
Erbe, C., Reichmuth, C., Cunningham, K., Lucke, K., and Dooling, R. (**2016**). "Communication masking in marine mammals: A review and research strategy," Mar. Pollut. Bull. **103**(1-2), 15–38.
European Union (**2008**). "Directive 2008/56/EC of the European Parliament and of the Council of 17 June 2008: Establishing a framework for community action in the field of marine environmental policy" (European Union, Brussels, Belgium).
Favali, P., Chierici, F., Marinaro, G., Giovanetti, G., Azzarone, A., Beranzoli, L., De Santis, A., Embriaco, D., Monna, S., Lo Bue, N., Sgroi, T., Cianchini, G., Badiali, L., Qamili, E., De Caro, M. G., Falcone, G., Montuori, C., Frugoni, F., Riccobene, G., Sedita, M., Barbagallo, G., Cacopardo, G., Cali, C., Cocimano, R., Coniglione, R., Costa, M., Amico, A., Del Tevere, F., Distefano, C., Ferrera, F., Giordano, V., Imbesi, M., Lattuada, D., Migneco, E., Musumeci, M. S., Orlando, A., Papaleo, R., Piattelli, P., Raia, G., Rovelli, A., Sapienza, P., Speziale, F., Trovato, A., Viola, S., Ameli, F., Bonori, M., Capone, A., Masullo, R., Simeone, F., Pignagnoli, L., Zitellini, N., Bruni, F., Gasparoni, F., and Pavan, G. (**2013**). "NEMO-SN1 abyssal cabled observatory in the Western Ionian Sea," IEEE J. Oceanic Eng. **38**(2), 358–374.
Frisk, G. (**1994**). *Ocean and Seabed Acoustics: A Theory of Wave Propagation* (PTR Prentice Hall, Englewood Cliffs, NJ), pp. 89–172.
Gisiner, R. C. (**2016**). "Sound and marine seismic surveys," Acoust. Today **12**(4), 10–18.
Guerra, M., Thode, A. M., Blackwell, S. B., Greene, C. R., Jr, and Macrander, M. (**2009**). "Quantifying masking effects of seismic survey reverberation off the Alaskan North Slope," J. Acoust. Soc. Am. **126**, 2230.
Guerra, M., Thode, A. M., Blackwell, S. B., and Michael Macrander, A. (**2011**). "Quantifying seismic survey reverberation off the Alaskan North Slope," J. Acoust. Soc. Am. **130**(5), 3046–3058.
Heaney, K. D., and Campbell, R. L. (**2019**). "Parabolic equation modeling of a seismic airgun array," IEEE J. Oceanic Eng. **44**(3), 621–632.
ISO (**2017**). ISO 18405:2017, "Underwater Acoustics—Terminology" (International Organization for Standardization, Geneva, Switzerland).
Laigle, M., and Sachpazi, M. (**2012**). "ULYSSE cruise, RV Pourquoi pas?".
MacGillivray, A. O. (**2006**). "Acoustic modelling study of seismic airgun noise in queen Charlotte basin," Ph.D. thesis, University of Victoria, Victoria, BC, Canada.
MacGillivray, A. O. (**2019**). "An airgun array source model accounting for high-frequency sound emissions during firing—Solutions to the IAMW source test cases," IEEE J. Oceanic Eng. **44**(3), 582–588.
MacGillivray, A. O., and Chapman, N. R. (**2012**). "Modeling underwater sound propagation from an airgun array using the parabolic equation method," Can. Acoust. **40**(1), 19–25.
MacGillivray, A. O., Racca, R., and Li, Z. (**2014**). "Marine mammal audibility of selected shallow-water survey sources," J. Acoust. Soc. Am. **135**(1), EL35–EL40.
Martin, S. B., Matthews, M. N. R., MacDonnell, J. T., and Bröker, K. (**2017**). "Characteristics of seismic survey pulses and the ambient soundscape in Baffin Bay and Melville Bay, West Greenland," J. Acoust. Soc. Am. **142**(6), 3331–3346.
Matthews, M. N. R., and MacGillivray, A. O. (**2013**). "Comparing modeled and measured sound levels from a seismic survey in the Canadian Beaufort Sea," Proc. Mtgs. Acoust. **19**(1), 070046.
Mattsson, A., and Jenkerson, M. (**2008**). "Single airgun and cluster measurement project," in *Joint Industry Programme (JIP) on Exploration and Production Sound and Marine Life Proramme Review*, pp. 28–30.
McCauley, R. D., Duncan, A. J., Gavrilov, A. N., and Cato, D. H. (**2016**). "Transmission of marine seismic survey, air gun array signals in Australian waters," in *Proceedings of Acoustics* (The Australasian Acoustical Societies, Brisbane, Australia), pp. 305–314.
McCauley, R. D., Fewtrell, J., Duncan, A. J., Jenner, C., Jenner, M. N., Penrose, J. D., Prince, R. I. T., Adhitya, A., Murdoch, J., and McCabe, K. (**2000**). "Marine seismic surveys—A study of environmental implications," APPEA J. **40**(1), 692–708.
McCauley, R. D., Meekan, M. G., and Parsons, M. J. (**2021**). "Acoustic pressure, particle motion, and induced ground motion signals from a commercial seismic survey array and potential implications for environmental monitoring," J. Mar. Sci. Eng. **9**(6), 571.
Moretti, P. F., and Affatati, A. (**2023**). "Understanding the impact of underwater noise to preserve marine ecosystems and manage anthropogenic activities," Sustainability **15**(13), 10178.
National Marine Fisheries Service (**2018**). "2018 revisions to: Technical guidance for assessing the effects of anthropogenic sound on marine mammal hearing (Version 2.0): Underwater Thresholds for onset of permanent and temporary threshold shifts," NOAA Technical Memorandum NMFS-OPR-59 (NOAA, Washington, DC), p. 167.
Nieukirk, S. L., Stafford, K. M., Mellinger, D. K., Dziak, R. P., and Fox, C. G. (**2004**). "Low-frequency whale and seismic airgun sounds recorded in the mid-Atlantic Ocean," J. Acoust. Soc. Am. **115**(4), 1832–1843.
Niu, H., Ozanich, E., and Gerstoft, P. (**2017**). "Ship localization in Santa Barbara Channel using machine learning classifiers," J. Acoust. Soc. Am. **142**(5), EL455–EL460.
Nowacek, D. P., Clark, C. W., Mann, D., Miller, P. J., Rosenbaum, H. C., Golden, J. S., Jasny, M., Kraska, J., and Southall, B. L. (**2015**). "Marine seismic surveys and ocean noise: Time for coordinated and prudent planning," Front. Ecol. Environ. **13**(7), 378–386.
Prior, M. K., Ainslie, M. A., Halvorsen, M. B., Hartstra, I., Laws, R. M., MacGillivray, A., Müller, R., Robinson, S., and Wang, L. (**2021**).

"Characterization of the acoustic output of single marine-seismic airguns and clusters: The Svein Vaage dataset," J. Acoust. Soc. Am. **150**(5), 3675–3692.
Przeslawski, R., Brooke, B., Carroll, A. G., and Fellows, M. (**2018**). "An integrated approach to assessing marine seismic impacts: Lessons learnt from the Gippsland Marine Environmental Monitoring project," Ocean Coastal Manage. **160**, 117–123.
Racca, R. G., and Scrimger, J. A. (**1986**). "Underwater acoustic source characteristics of air and water guns," Contractor report by JASCO Res. Ltd., Victoria BC DREP Contract (**06SB**), 97708–97705 (JASCO, Victoria, BC, Canada).
Sciacca, V., Morello, G., Beranzoli, L., Embriaco, D., Filiciotto, F., Marinaro, G., Riccobene, G. M., Simeone, F., and Viola, S. (**2023**). "Song notes and patterns of the Mediterranean Fin Whale (*Balaenoptera physalus*) in the Ionian Sea," J. Mech. Sci. Eng. **11**(11), 2057.
Sciacca, V., Viola, S., Pulvirenti, S., Riccobene, G., Caruso, F., De Domenico, E., and Pavan, G. (**2016**). "Shipping noise and seismic airgun surveys in the Ionian Sea: Potential impact on Mediterranean fin whale," Proc. Mtgs. Acoust. **27**(1), 040010.
Seri, S. G., Zhu, C., Schinault, M., Garcia, H., Handegard, N. O., and Ratilal, P. (**2019**). "Long range passive ocean acoustic waveguide remote sensing (POAWRS) of seismo-acoustic airgun signals received on a coherent hydrophone array," in *Proceedings of Oceans 2019, MTS/IEEE*, Seattle, WA, pp. 1–8.
Sigray, P., Andersson, M., Andre, M., Azzellino, A., Borsani, J., Bou, M., Castellote, M., Ceyrac, L., Dellong, D., Folegot, T., Hedgeland, D., Juretzek, C., Klauson, A., Leaper, R., Le Courtois, F., Liebschner, A., Maglio, A., Müller, A., Norro, A., Novellino, A., Outinen, O., Popit, A., Prospathopoulos, A., Thomsen, F., Tougaard, J., Vukadin, P., and Weilgart, L. (**2023**). *Setting EU Threshold Values for Impulsive Underwater Sound*, edited by J. Druon, G. Hanke, and M. Casier (Publications Office of the European Union, Luxembourg).
Southall, B. L., Donovan, G. P., Racca, R., Reeves, R. R., Vedenev, A. I., Weller, D. W., and Nowacek, D. P. (**2023**). "Data collection and analysis methods to evaluate potential impacts of seismic surveys and other marine industrial activities on baleen whales," Ocean Coastal Manage. **245**, 106799.
Viola, S., Grammauta, R., Sciacca, V., Bellia, G., Beranzoli, L., Buscaino, G., Caruso, F., Chierici, F., Cuttone, G., D'Amico, A., De Luca, V., Embriaco, D., Favali, P., Giovanetti, G., Marinaro, G., Mazzola, S., Filiciotto, F., Pavan, G., Pellegrino, C., Pulvirenti, S., Simeone, F., Speziale, F., and Riccobene, G. (**2017**). "Continuous monitoring of noise levels in the Gulf of Catania (Ionian Sea). Study of correlation with ship traffic," Mar. Pollut. Bull. **121**(1–2), 97–103.
Vitard, C. (**2016**). "Investigation sismique du domaine avant-arc Égéen du segment Sud-Ouest de la zone de subduction Hellénique," "(Seismic investigation of the Aegean forearc domain of the southwest segment of the Hellenic subduction zone)", Ph.D. thesis, Université Côte d'Azur, Nice, France.
Wiggins, S. M., Hall, J. M., Thayre, B. J., and Hildebrand, J. A. (**2016**). "Gulf of Mexico low-frequency ocean soundscape impacted by airguns," J. Acoust. Soc. Am. **140**(1), 176–183.
Zhang, Z. Y., and Tindle, C. T. (**1995**). "Improved equivalent fluid approximations for a low shear speed ocean bottom," J. Acoust. Soc. Am. **98**(6), 3391–3396.
Ziolkowski, A. (**1970**). "A method for calculating the output pressure waveform from an air gun," Geophys. J. Int. **21**(2), 137–161.
Ziolkowski, A., Parkes, G., Hatton, L., and Haugland, T. (**1982**). "The signature of an air gun array; computation from near-field measurements including interactions," Geophysics **47**(10), 1413–1421.